Human Molecular Genetics, 2010, Vol. 19, No. 18 **3491–3501**
doi:10.1093/hmg/ddq265
Advance Access published on June 29, 2010

CHD7 functions in the nucleolus as a positive regulator of ribosomal RNA biogenesis

Gabriel E. Zentner[1], Elizabeth A. Hurd[5], Michael P. Schnetz[1], Lusy Handoko[7], Chuanping Wang[2], Zhenghe Wang[1,3], Chialin Wei[7], Paul J. Tesar[1,4], Maria Hatzoglou[2], Donna M. Martin[5,6] and Peter C. Scacheri[1,3,*]

[1]Department of Genetics, [2]Department of Nutrition, [3]Case Comprehensive Cancer Center and [4]Center for Stem Cell and Regenerative Medicine, Case Western Reserve University, Cleveland, OH 44106, USA, [5]Department of Pediatrics and [6]Department of Human Genetics, University of Michigan, Ann Arbor, MI 48109, USA and [7]Genome Technology and Biology Group, Genome Institute of Singapore, 138672, Singapore, Singapore

Received March 29, 2010; Revised June 14, 2010; Accepted June 23, 2010

De novo **mutation of the gene encoding chromodomain helicase DNA-binding protein 7 (CHD7) is the primary cause of CHARGE syndrome, a complex developmental disorder characterized by the co-occurrence of a specific set of birth defects. Recent studies indicate that CHD7 functions as a transcriptional regulator in the nucleoplasm. Here, we report based on immunofluorescence and western blotting of subcellular fractions that CHD7 is also constitutively localized to the nucleolus, the site of rRNA transcription. Standard chromatin immunoprecipitation (ChIP) assays indicate that CHD7 physically associates with rDNA, a result that is also observable upon alignment of whole-genome CHD7 ChIP coupled with massively parallel DNA sequencing data to the rDNA reference sequence. ChIP-chop analyses demonstrate that CHD7 specifically associates with hypomethylated, active rDNA, suggesting a role as a positive regulator of rRNA synthesis. Consistent with this hypothesis, siRNA-mediated depletion of CHD7 results in hypermethylation of the rDNA promoter and a concomitant reduction of 45S pre-rRNA levels. Accordingly, cells overexpressing CHD7 show increased levels of 45S pre-rRNA compared with control cells. Depletion of CHD7 also reduced cell proliferation and protein synthesis. Lastly, compared with wild-type ES cells, the levels of 45S pre-rRNA are reduced in both *Chd7*$^{+/-}$ and *Chd7*$^{-/-}$ mouse ES cells, as well as in *Chd7*$^{-/-}$ whole mouse embryos and multiple tissues dissected from *Chd7*$^{+/-}$ embryos. Together with previously published studies, these results indicate that CHD7 dually functions as a regulator of both nucleoplasmic and nucleolar genes and provide a novel avenue for investigation into the pathogenesis of CHARGE syndrome.**

INTRODUCTION

The chromodomain helicase DNA-binding (CHD) protein family is a highly conserved group of nuclear proteins with nine members in vertebrates (reviewed in 1,2). Although the cellular functions of the CHD proteins are suspected to be quite diverse, roles in transcriptional regulation are emerging as a common theme. CHD1, for example, was recently shown to regulate ES cell pluripotency genes including *Oct4* (3). CHD3 and CHD4 (also known as Mi-2α and Mi-2β) are integral components of the nucleosome remodeling and deacetylating complex (4), involved in transcriptional repression. CHD5 is a tumor suppressor that controls cell growth and apoptosis by positively regulating p53 target genes including *p21* and *Bax* (5). CHD8 controls cell cycle progression by regulating the cyclin E2 gene (6) and has also been shown to regulate the transcription of β-catenin target genes (7).

Of all nine CHD proteins, CHD7 is of particular interest. *De novo* mutation of the *CHD7* gene gives rise to CHARGE syndrome, a complex genetic condition characterized by Coloboma of the eye, Heart malformations, Atresia of the choanae, Retardation of growth, Genital hypoplasia and Ear

*To whom correspondence should be addressed at: 2109 Adelbert Road, Cleveland, OH 44106, USA. Tel: +1 2163683458; Fax: +1 2163683432; Email: peter.scacheri@case.edu

abnormalities and deafness (8). Other clinical features not included in the acronym include tracheoesophagal fistula, anosmia and limb anomalies (9–11). Approximately two-thirds of the cases of CHARGE syndrome are due to mutation of *CHD7* (8). Most *CHD7* mutations are nonsense or frameshift and predicted to be loss of function, and thus haploinsufficiency is hypothesized to be the pathogenic mechanism. Studies in mice support the haploinsufficiency model. Specifically, mice that are heterozygous for a W973X nonsense mutation in the *Chd7* gene, also known as *Whirligig*, display many of the features of human CHARGE syndrome, including postnatal growth retardation, choanal atresia, inner ear malformations, female genital hypoplasia, heart defects and olfactory defects (12,13). Gene-trap technology has also been used to generate *Chd7* mutant mice, and $Chd7^{Gt/+}$ mice develop a phenotype similar to *Whirligig* mice (14). Mice that are homozygous for either the *Whirligig* or gene-trap alleles die by embryonic day 11 (12,14). *In situ* hybridization and immunofluorescence analyses of mouse embryos at multiple stages of embryonic development indicate that *Chd7* expression is spatially and temporally dynamic, suggesting that the requirements for CHD7 during development are specific to both tissue and stage (11,12,14).

To gain insight into the function of CHD7, we recently mapped the distribution of CHD7 on chromatin using the approaches of chromatin immunoprecipitation coupled with microarray analysis (ChIP-chip) or massively parallel DNA sequencing (ChIP-seq) (15,16). In multiple cell types, hundreds to thousands of CHD7 sites were identified. Most of the CHD7 sites show features of gene-enhancer elements. Specifically, CHD7 sites were predominantly located distal to transcription start sites, shown to correlate with cell-specific gene expression and found within open regions of chromatin marked with H3K4 monomethylation, the epigenetic signature of enhancers. Moreover, in ES cells, CHD7 was found to co-localize with p300, a known enhancer-binding protein and strong predictor of enhancer activity. Despite the strong correlation with enhancer elements, most genes directly targeted by CHD7 were only subtly altered (<2-fold) in expression in $Chd7^{+/-}$ and $Chd7^{-/-}$ ES cells. These studies are consistent with a role for CHD7 as a transcriptional regulator, suggesting that dysregulated gene expression contributes to the pathogenesis of CHARGE syndrome. However, it is not yet clear whether subtle changes in gene expression are sufficient to give rise to CHARGE syndrome, or if the genes normally targeted by CHD7 are more dramatically affected by CHD7 deficiency at later stages of development.

Virtually all CHD proteins have been reported to localize to the nucleoplasm. A search of the Nucleolar Proteome Database (17) shows that all nine CHD proteins have also been detected in the nucleolus via proteomic methods. These studies raise the possibility that CHD proteins, in addition to functioning as regulators of nuclear gene expression, dually function as regulators of rRNA biogenesis. Consistent with this hypothesis, CHD4, a repressor of nuclear gene transcription, was shown to associate with rDNA and activate rRNA transcription (18). In this report, we confirm that CHD7 localizes to the nucleolus and binds to transcriptionally active rDNA. We present evidence that both haploinsufficiency and complete loss of CHD7 lead to increased DNA methylation of the rRNA promoter, resulting in decreased rRNA expression. We also show that CHARGE-affected tissues isolated from heterozygous *Chd7* mouse embryos have reduced levels of rRNA. The results presented herein delineate a novel, nucleolar function for CHD7 and also raise the possibility that CHARGE syndrome arises through dysregulation of nucleoplasmic and nucleolar genes.

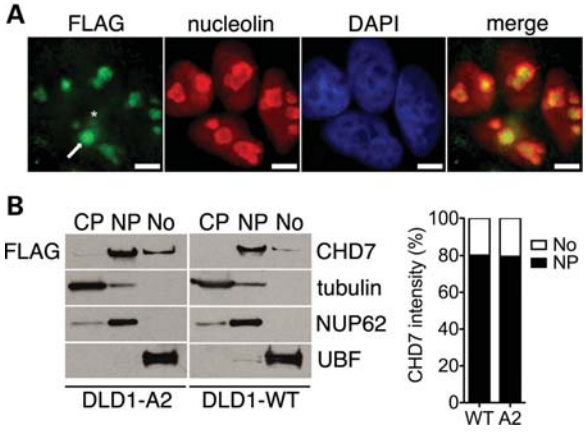

Figure 1. CHD7 localizes to the nucleoplasm and nucleolus. (**A**) Immunofluorescent staining of DLD1-A2 cells with FLAG and nucleolin antibodies. The arrow indicates nucleolar localization of CHD7, whereas the asterisk marks nucleoplasmic CHD7. Scale bar = 4 μm. (**B**) Western blot analysis of subcellular fractions from DLD1-A2 and DLD1-WT cells. The purity of cytoplasmic (CP), nucleoplasmic (NP) and nucleolar (No) fractions was assessed by blotting for tubulin, NUP62 and UBF, respectively. Densitometric quantification of CHD7 in the nucleoplasmic and nucleolar fractions is also shown and expressed as a percentage of total CHD7 signal.

RESULTS

CHD7 is dually localized to the nucleoplasm and nucleolus

To facilitate immunodetection of CHD7, we took advantage of a human colorectal cancer cell line, DLD1, in which DNA encoding three FLAG epitopes have been knocked-in to the 3′ end of the *CHD7* gene, resulting in the expression of epitope-tagged CHD7 under the control of its endogenous promoter (19) (hereafter referred to as DLD1-A2). Importantly, previous ChIP-chip studies have shown that the distribution of the epitope-tagged form of CHD7 on chromatin is similar to that of the untagged form, indicating that the presence of the FLAG tag does not overtly affect the function of CHD7 (15, 19). As expected, immunofluorescent staining with FLAG antibodies showed CHD7 in the nucleus. However, high levels of CHD7 were also detected in the nucleolus. Nucleolar localization CHD7 was validated by co-staining with nucleolin, an abundant eukaryotic nucleolar protein (20) (Fig. 1A). Quantification of CHD7 immunofluorescence revealed that, on average, 60% of CHD7 was nucleoplasmic, whereas the remaining 40% was nucleolar, though a significant degree of cell–cell variability was observed (Supplementary Material, Fig. S1A and B). All cells examined showed co-localization of CHD7 and nucleolin ($n = 107$), indicating that the nucleolar localization of CHD7 is constitutive. Nucleolar localization of CHD7 was further validated by CHD7 western blot analysis of subcellular fractions isolated

from both epitope-tagged and wild-type DLD1 cells, indicating that the immunofluorescence results are not artifactual or due to the presence of the FLAG tag. Densitometric quantification of these blots showed that ~20% of cellular CHD7 is localized to the nucleolus, whereas the remaining ~80% is nucleoplasmic (Fig. 1B).

CHD7 associates with rDNA

Mammalian cells contain several hundred tandemly duplicated rRNA genes, clustered into repeated arrays known as nucleolar organizer regions (NORs) (21). Human NORs are located on the p-arms of the five acrocentric chromosomes (13, 14, 15, 21 and 22) (22), while mouse NORs are located on chromosomes 12, 15, 17, 18 and 19 (23). rRNA genes are approximately 42.9 kb in length in humans and 45 kb in mice and contain approximately 13–14 kb of coding sequence with the remainder made up by the non-coding intergenic spacer region (Fig. 2A). To determine whether CHD7 directly associates with rDNA, we performed ChIP analyses with multiple primer sets designed to amplify several regions within the coding and non-coding regions of rDNA. These studies were carried out in both human DLD1-A2 cells and in mouse ES (mES) cells, which express high levels of CHD7. We detected a high enrichment of CHD7 at multiple sites along the rDNA loci in both DLD1-A2 and mES cells (Fig. 2B and C). The relative pattern of CHD7 occupancy at rDNA loci differed between the two cell types tested. Specifically, while CHD7 binds to the coding region of the rDNA in DLD1-A2 cells, binding occurs at the promoter and the 3′ end of the coding sequence in mES cell rDNA. The reason for these differences is currently not clear, but might reflect species or cell type-specific differences. Indeed, UBF occupancy at rDNA has been shown to vary between the Jurkat cell line and the Kasumi and HEL lines (24). In addition, transcription factors involved in cell lineage differentiation such as Runx2, MyoD and Mgn have been found to differentially occupy rDNA in undifferentiated C2C12 cells versus cells differentiating along muscle, bone and adipose lineages (25).

We recently mapped the distribution of CHD7 on chromatin using the approach of ChIP-seq. These studies were carried out in both DLD1-A2 and mES cells (16 and M.P.S. and P.C.S., unpublished data). Although thousands of CHD7 sites were detected on nucleoplasmic chromatin, the reference genome assemblies to which the ChIP-seq data were aligned do not contain the rDNA loci, and therefore CHD7 occupancy at rDNA was not assessed. In this study, we realigned the CHD7 ChIP-seq data to rDNA reference sequences. The results show a high enrichment of CHD7 at the rDNA in a pattern that is generally consistent with that determined by ChIP–PCR (Fig. 2D and E). The ChIP-seq results not only validate the signals observed by ChIP–PCR, but also suggest that ChIP-seq is a viable technology for the analysis of proteins bound to rDNA, as previously shown for UBF (26).

CHD7 influences the levels of the 45S pre-rRNA

rDNA is transcribed by RNA polymerase I (RNA pol I) into a 45S pre-rRNA that undergoes a complex series of RNase cleavage and chemical modification steps to yield the mature

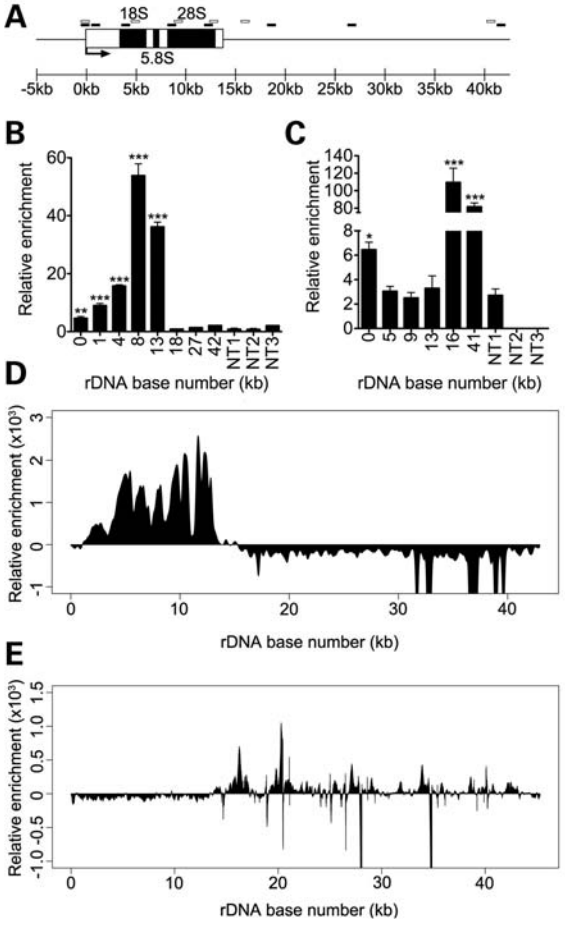

Figure 2. CHD7 binds to rDNA. (**A**) Schematic representation of a mammalian rDNA repeat. Approximate locations of qPCR primers for human ChIP are denoted by black boxes and mouse ChIP by open boxes. (**B**) ChIP–PCR analysis of FLAG-CHD7 binding to the human rDNA locus. (**C**) ChIP–PCR analysis of CHD7 binding to the mouse rDNA locus. For ChIP–PCR, non-target regions are included as controls for specificity of CHD7 enrichment. Error bars represent the mean + SD for triplicates. ChIP-seq of FLAG-CHD7 at human rDNA in DLD1-A2 cells (**D**) and mouse rDNA in mES cells (**E**) recapitulates the binding patterns of CHD7 seen by ChIP–PCR. $^{*}P < 0.05$; $^{**}P < 0.01$; $^{***}P < 0.001$ by *t*-test versus non-target regions.

28S, 18S and 5.8S rRNA species that are then assembled into mature ribosomes (reviewed in 27). Having established that CHD7 binds to rDNA, we next investigated if CHD7 plays a role in regulating rRNA levels. Specifically, we performed siRNA knockdown of CHD7 in DLD1-A2 cells (Fig. 3A), followed by qRT–PCR of the human 45S pre-rRNA. Compared with cells transfected with non-specific control siRNAs, two independent CHD7 siRNAs reduced pre-rRNA levels 20–30% (Fig. 3B). We also quantified the levels of the 45S pre-rRNA in *Chd7* wild-type, heterozygous and null mES cells derived from *Whirligig* mouse embryos (12), which harbor a nonsense mutation in the *Chd7* gene and express levels of *Chd7* consistent with their genotypes (Fig. 3C). Compared with wild-type cells, $Chd7^{+/-}$ and $Chd7^{-/-}$ mES cells show a significant reduction in pre-rRNA levels (Fig. 3D). The level of the pre-rRNA in $Chd7^{+/-}$ ES cells is halfway

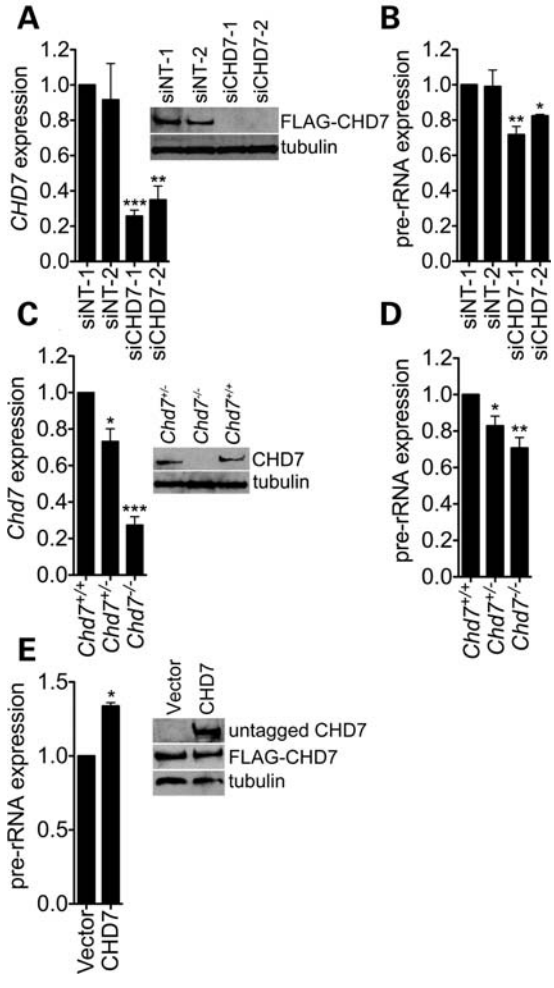

Figure 3. CHD7 positively regulates rRNA transcription. (**A**) qRT–PCR and western blot analysis of CHD7 mRNA and protein levels following the treatment of DLD1-A2 cells with non-target siRNA pools (siNT-1/2), a CHD7 siRNA pool (siCHD7-1) and a CHD7 siRNA not present in the pool (siCHD7-2). (**B**) qRT–PCR for the 45S pre-rRNA in cells treated with control or CHD7 siRNA ($n = 2–5$). (**C**) qRT–PCR and western blot analysis of CHD7 mRNA and protein levels in mES cells derived from *Whirligig* embryos. (**D**) qRT–PCR for the 45S pre-rRNA in mES cells ($n = 4–7$). (**E**) qRT–PCR analysis of 45S pre-rRNA levels in DLD1-A2 cells transfected with empty vector or plasmid encoding untagged human CHD7 protein ($n = 2$). The FLAG-tagged CHD7 expressed in DLD1-A2 cells is not detectable with the Abcam CHD7 antibody and thus, blotting with this antibody only reveals the untagged CHD7 that was transfected (see Supplementary Material, Fig. S2). Error bars represent mean + SEM for biological replicates. $^{*}P < 0.05$; $^{**}P < 0.01$; $^{***}P < 0.001$ by *t*-test.

between that of the wild-type and null cells, indicating that the effect of *Chd7* deficiency on rRNA is dosage-sensitive.

Having established that reduced levels of CHD7 result in decreased levels of the 45S pre-rRNA, we next tested whether increased expression of CHD7 would have the opposite effect on pre-rRNA levels. Specifically, we transiently transfected DLD1-A2 cells with a construct encoding full-length CHD7 and quantified the levels of the 45S pre-rRNA. Compared with cells transfected with empty vector, cells overexpressing CHD7 showed ~33% higher levels of 45S pre-rRNA (Fig. 3E). These results indicate that the modulation of CHD7 in either the positive or the negative direction results in concomitant changes in the expression of the 45S pre-rRNA. Together with the CHD7 ChIP data indicating an association of CHD7 with rDNA, these results suggest that CHD7 likely directly regulates transcription of the rDNA; however, we currently cannot rule out the possibility that CHD7 influences early rRNA processing events.

Depletion of CHD7 reduces cell proliferation and protein synthesis

Having established that CHD7 functions as a positive regulator of rRNA synthesis, we next chose to investigate the cellular effects of CHD7 knockdown. We first chose to assay cell proliferation, as alterations in the levels of rRNA regulators are known to influence cell growth and proliferation (28–30). We performed siRNA knockdown of CHD7 in DLD1-A2 cells and performed cell counting each day for 5 days following knockdown. A significant reduction in cell number was observed 5 days post-siRNA transfection (Fig. 4A). To determine the cause of the reduction in cell number, we quantified BrdU-labeled DLD1-A2 cells treated with control or CHD7 siRNA 5 days post-transfection. A significant reduction in the number of BrdU-positive cells was observed in the CHD7 siRNA-treated group (Fig. 4B and C). We therefore conclude that knockdown of CHD7 inhibits cell proliferation, consistent with its function as a positive regulator of rRNA synthesis.

In addition to influencing cell proliferation, rRNA synthesis is rate-limiting for ribosome biogenesis (31). We therefore tested whether the depletion of CHD7 affected global protein synthesis. We performed siRNA-mediated knockdown of CHD7 in DLD1-A2 cells and performed metabolic labeling with [^{35}S]methionine at 3, 4 and 5 days after siRNA transfection. A significant reduction in radiolabeled methionine incorporation was seen 4 days after knockdown (Fig. 4D), suggesting that the impairment of rRNA synthesis caused by CHD7 depletion impairs protein synthesis. Global protein synthesis recovers to near wild-type levels 5 days post-transfection, though the CHD7 siRNA is still effective at this time point (Fig. 4E). However, at this time, cells show a proliferation defect. It is currently not clear why a defect in protein synthesis occurring 4 days post-transfection gives rise to a proliferation defect 5 days post-transfection; however, one potential explanation is that compensatory mechanisms have been engaged to restore protein synthesis by day 5 post-transfection but are not sufficient to restore normal cell proliferation. Further studies are required to test this hypothesis.

We next tested whether the cell proliferation defect observed in CHD7 siRNA-treated cells could be due to stabilization of p53, which has been reported to be induced upon nucleolar stress (32). Compared with control-treated cells, p53 protein levels remained unchanged three through 5 days following CHD7 knockdown (Fig. 4E). Alterations in *p53* transcript levels were also not detected (Fig. 4F). We next tested whether *p21* transcript levels were altered, as p21 is a well-known cell cycle inhibitor that can also be induced by cellular stress, either in a p53-dependent or independent fashion (33–37). The results of qRT–PCR analyses showed a significant increase in the levels of *p21* following CHD7

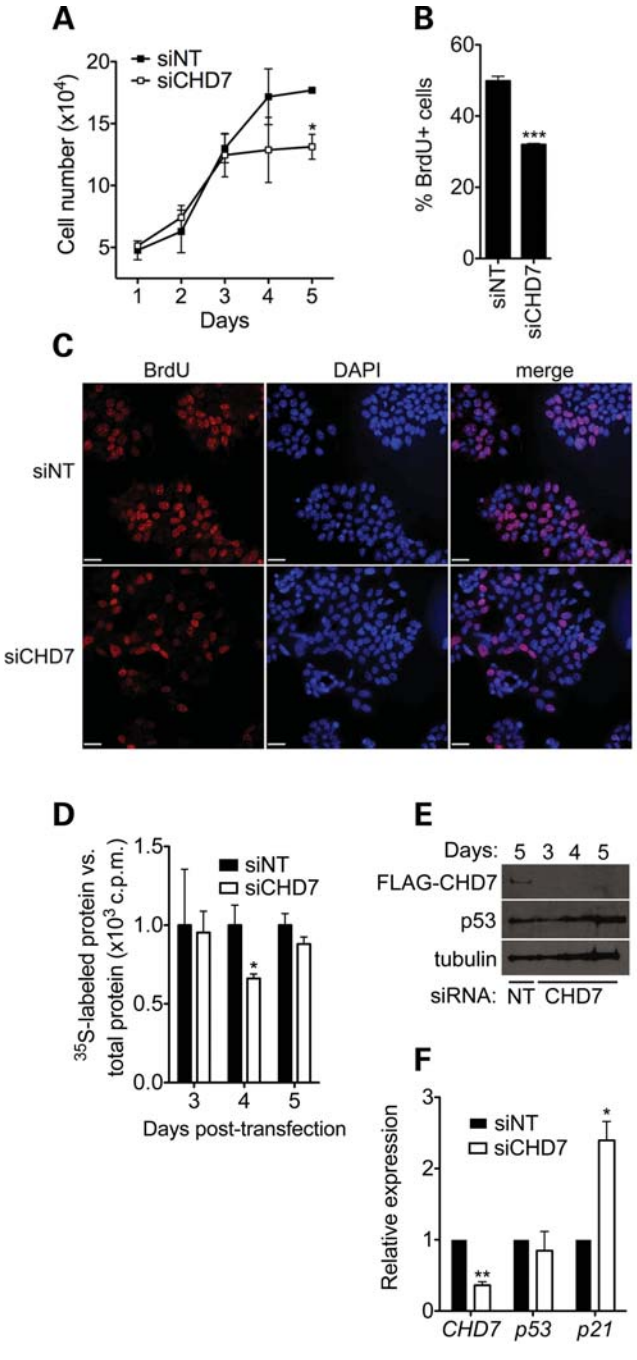

Figure 4. Loss of CHD7 impairs cell proliferation and protein synthesis. (**A**) Cell counting assay performed in DLD1-A2 cells treated with the indicated siRNA. Error bars represent mean + SD ($n = 3$). (**B**) Quantification of BrdU labeling 5 days post-transfection in DLD1-A2 cells treated with control or CHD7 siRNA. Error bars represent mean + SEM ($n = 2–3$). (**C**) Representative image of BrdU labeling in control and BrdU labeling in DLD1-A2 cells showing a qualitative reduction in labeling in CHD7 siRNA-treated cells. Fields are approximately matched for cell number (160–180 cells/field). Scale bar = 32 μm. (**D**) Measurement of global protein synthesis in DLD1-A2 cells after CHD7 knockdown by [^{35}S]methionine radiolabeling at the indicated time points after siRNA transfection. Scintillation counts were normalized to total protein. (**E**) Western blots of FLAG-CHD7 and p53 in DLD1-A2 cells. These blots indicate that the CHD7 siRNA is effective up to 5 days post-transfection and that p53 protein levels are not altered. (**F**) qRT–PCR analysis of *CHD7*, *p53* and *p21* transcript levels in DLD1-A2 cells 4 days post-transfection with siRNA ($n = 4$). $^{*}P < 0.05$; $^{**}P < 0.01$; $^{***}P < 0.001$ by *t*-test.

knockdown (Fig. 4F). These results suggest that upregulation of p21 may contribute to proliferation defects observed in the CHD7 knockdown cells, although future studies are required to test whether the upregulation of p21 is due to nucleolar stress, or dysregulation of CHD7-mediated transcription in the nucleoplasm.

CHD7 antagonizes DNA methylation at active rDNA repeats

rDNA repeats are maintained in two distinct epigenetic states (21). Active repeats have a euchromatic structure, characterized by methylation of H3K4, acetylation of H3 and H4 and relatively low levels of CpG methylation. Inactive repeats have a heterochromatic structure, with higher levels of CpG methylation, methylation of H3K9 and H4K20 and hypoacetylation of H4 (Fig. 5A). Proteins that bind to rDNA may be specific for active or inactive repeats (38), potentially providing insight into their function at rDNA repeats. Because reduced CHD7 levels correlate with reduced levels of 45S pre-rRNA, we hypothesized that CHD7 is a positive regulator of rDNA transcription and as such might associate with active rDNA repeats. To address this possibility, we used the ChIP-chop assay (38). Specifically, ChIP was performed on chromatin from DLD1-A2 cells using antibodies to FLAG-CHD7, H3K4me2 (predominantly found at active rDNA repeats) and H3K9me2 (predominantly found at inactive rDNA repeats). Chromatin from input and ChIP samples was then digested with *Hpa*II, a methylation-sensitive enzyme that does not cut the internal CpG within the sequence CCGG if it is methylated. Primer pairs flanking *Hpa*II sites within the human rDNA repeat were then used to amplify mock- and *Hpa*II-digested DNA. DNA immunoprecipitated by FLAG-CHD7 showed a level of *Hpa*II resistance more similar to that of H3K4me2 than H3K9me2, suggesting that CHD7 predominantly associates with unmethylated, active rDNA repeats in DLD1-A2 cells (Fig. 5B).

We next investigated whether the loss of CHD7 was associated with changes in the epigenetic state of rDNA repeats. We chose to assay DNA methylation of the rDNA promoter, as it has a well-established role in the silencing of rRNA expression (21). Genomic DNA was isolated from DLD1-A2 cells treated with either control or CHD7 siRNA, digested with *Hpa*II and PCR-amplified using primers flanking the rDNA promoter. The rDNA promoter in CHD7-siRNA-treated cells was significantly more resistant to *Hpa*II digestion than control promoter DNA, indicating an increase in promoter methylation upon reduction in CHD7 levels (Fig. 5C). Similar results were observed in comparisons between $Chd7^{+/+}$, $Chd7^{+/-}$ and $Chd7^{-/-}$ ES cells (Fig. 5D). To ensure that the increase in *Hpa*II resistance was due to internal CpG methylation rather than methylation of the external C residue of the recognition sequence, the same genomic DNA was also digested with *Msp*I, an isoschizomer of *Hpa*II. *Msp*I cleaves the CCGG sequence regardless of the methylation status of the internal C but will not cut if the external C is methylated. Genomic DNA that was resistant to *Hpa*II showed little resistance to *Msp*I cleavage, indicating that the majority of methylation at the assayed CCGG sites is on the internal CpG (Fig. 5C

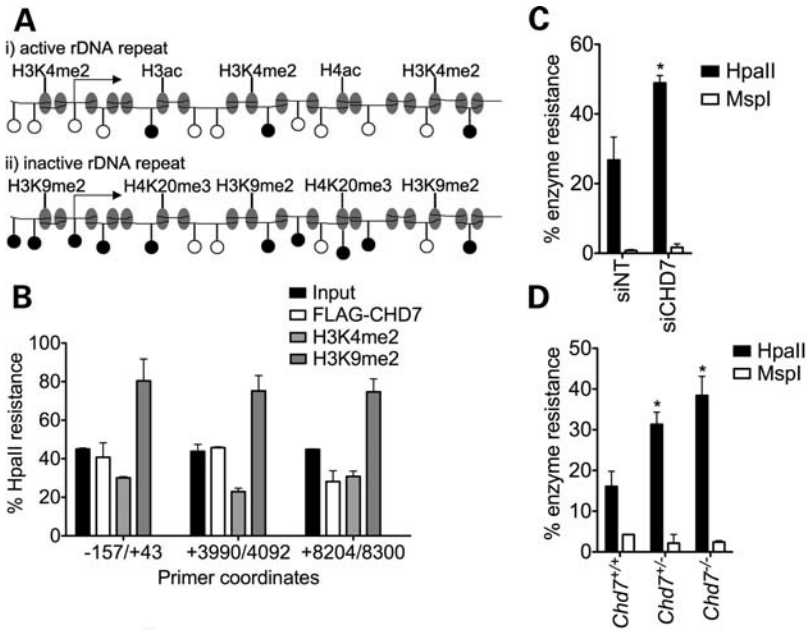

Figure 5. CHD7 is associated with active rDNA repeats and counteracts rDNA promoter methylation. (**A**) Schematic representation of active and inactive rDNA loci showing their respective epigenetic features. Open circles represent unmethylated CpG dinucleotides and methylated CpG dinucleotides are represented as filled circles. (**B**) ChIP-chop analysis of FLAG-CHD7, H3K4me2 and H3K9me2 binding to the human rDNA locus in DLD1-A2 cells ($n = 2$). (**C**) Analysis of rDNA promoter methylation in DLD1-A2 cells by *Hpa*II/*Msp*I digest and qPCR ($n = 3$). (**D**) Analysis of rDNA promoter methylation in mES cells by *Hpa*II/*Msp*I digest and qPCR ($n = 3$). Error bars represent the mean + SEM for biological replicates. $^{*}P < 0.05$ by *t*-test.

and D). These results suggest that CHD7 either initiates or maintains the expression of rRNA by associating with active rDNA loci and that loss of CHD7 results in the conversion of active rDNA to a more heterochromatic state.

CHARGE-relevant tissues from *Chd7* gene-trap mice show reduced pre-rRNA levels

Having established a role for CHD7 in rRNA biogenesis in two cell culture models, we next sought to examine the relevance of these results to a model of CHARGE syndrome. Similar to *Whirligig* mice, *Chd7* gene-trap mice ($Chd7^{Gt/+}$) display several features of human CHARGE syndrome including inner ear defects, postnatal growth retardation and hyposmia (11,14). $Chd7^{Gt/+}$ mice were bred and whole embryos were harvested at E9.5, just prior to the time at which $Chd7^{Gt/Gt}$ embryos die. We then performed qRT–PCR for the 45S pre-rRNA on total RNA isolated from whole embryos. Compared with wild-type embryos, $Chd7^{Gt/Gt}$ embryos showed a significant reduction in the levels of the 45S pre-rRNA. The levels of the 45S pre-rRNA were similar between wild-type and $Chd7^{Gt/+}$ embryos (Fig. 6A). The discrepancy between the results observed in the homozygous and heterozygous embryos could be related to differences in the severity of the phenotypes, i.e. $Chd7^{Gt/Gt}$ embryos die in mid-gestation, whereas $Chd7^{Gt/+}$ mice are viable. Alternatively, the lack of aberrant pre-rRNA expression in heterozygotes may be related to the fact that only a subset of organs are affected in the mouse, and the effect on the pre-rRNA is masked when the whole embryo is analyzed.

To test whether the role of CHD7 in pre-rRNA synthesis is tissue-specific, we dissected otocyst, eye, heart and limb tissue from $Chd7^{+/+}$ and $Chd7^{Gt/+}$ embryos at E10.5 and quantified pre-rRNA levels by qRT–PCR. Despite the inherent limitations of quantifying expression across ostensibly variable samples (Fig. 6B), we detected a significant reduction in pre-rRNA expression in $Chd7^{Gt/+}$ eye and ear tissues (Fig. 6C). In contrast, $Chd7^{Gt/+}$ heart and limb tissues were comparable to wild-type levels. These results could be indicative of cell type or developmental stage-specific nucleolar roles for CHD7. Interestingly, the degree of pre-rRNA reduction appears to correlate with the penetrance of tissue-specific malformations. Inner ear defects are observed in all $Chd7^{Gt/+}$ mice (14) and keratoconjunctivitis sicca is observed in ~50% of *Whirligig* mice (12). Cardiac malformations have been identified in a small number of *Whirligig* mice (12), and limb defects in *Chd7* mutants have not yet been characterized.

CHD7 promotes rDNA association of the Treacher Collins syndrome protein, treacle

Treacher Collins syndrome (TCS) is a congenital multiple anomaly disorder characterized predominantly by craniofacial anomalies (39). TCS is caused by *de novo* mutations in *TCOF1*, encoding treacle. Intriguingly, treacle is a nucleolar protein that specifically associates with rDNA and functions as a positive regulator of rRNA synthesis (40). Although TCS and CHARGE are clearly clinically distinct syndromes, several organ systems are affected in both conditions, including the eyes and ears. Based on these observations and the data presented here indicating that CHD7 also functions in rRNA synthesis, we tested whether CHD7 and treacle co-associate at rDNA. ChIP analysis of treacle in *Chd7* wild-type and null cells demonstrated that the absence of CHD7 impaired

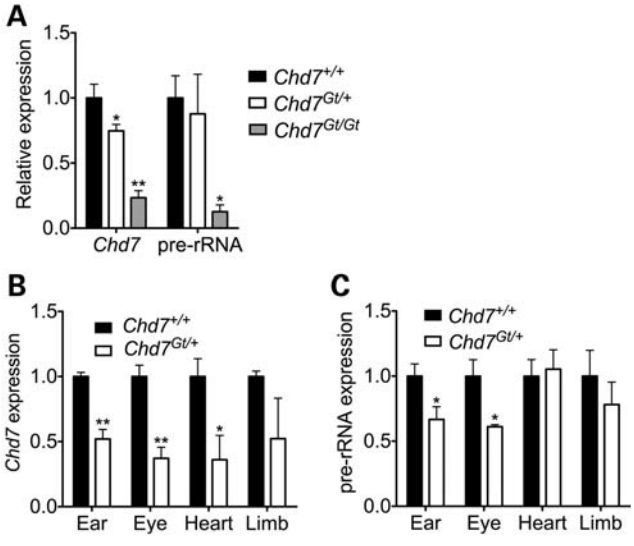

Figure 6. Pre-rRNA levels are reduced in embryonic *Chd7* mutant CHARGE tissues. (**A**) qRT–PCR for *Chd7* and pre-rRNA in whole E10.5 *Chd7* gene-trap embryos ($n = 2–3$). (**B**) qRT–PCR for the 45S pre-rRNA in *Chd7* mutant tissues. (**C**) qRT–PCR for the 45S pre-rRNA in *Chd7* mutant tissues. Error bars represent the mean + SEM for biological replicates ($n = 3–4$). $^{*}P < 0.05$, $^{**}P < 0.01$ by *t*-test.

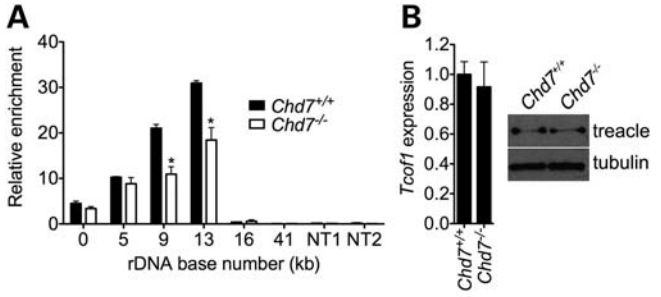

Figure 7. CHD7 promotes association of treacle with rDNA. (**A**) ChIP analysis of treacle binding to rDNA in $Chd7^{+/+}$ and $Chd7^{-/-}$ mES cells ($n = 2$). Two nucleoplasmic non-target regions are included as controls for ChIP specificity. (**B**) qRT–PCR and western blot analysis of *Tcof1* mRNA and treacle protein levels, respectively, in $Chd7^{+/+}$ and $Chd7^{-/-}$ mES cells ($n = 3$). Error bars represent the mean + SEM for biological replicates. $^{*}P < 0.05$ by *t*-test.

the ability of treacle to bind rDNA (Fig. 7A). This result was not due to alterations in the expression of *Tcof1* or treacle protein stability as assayed by qRT–PCR and western blot (Fig. 7B). These findings suggest that the association of treacle with rDNA is partially dependent on the presence of CHD7 and raise the possibility of a functional connection between the two proteins and the pathogenesis of CHARGE and TCS. *In vivo* studies involving breeding of *Chd7* and *Tcof1* mutant mice could be used to further investigate this possibility.

DISCUSSION

Previous studies indicate that CHD7 binds to gene-enhancer elements and functions as a transcriptional regulator in the nucleoplasm. Here, we provide evidence that CHD7 also functions in the nucleolus as a positive regulator of rRNA biogenesis. Depletion of CHD7 through siRNA or genetic mutation results in a 20–30% reduction in pre-rRNA levels. Though this effect appears relatively small, it is important to consider the sheer volume of cellular transcription accounted for by rRNA. rRNA transcription accounts at least 50% of overall cellular transcription in most growing eukaryotic cells (41), and it thus stands to reason that what appears to be a relatively modest effect on rRNA transcription may in fact have large biological impact. Consistent with this notion, we detected reductions in pre-rRNA levels in two frequently affected tissues from *Chd7* heterozygous mice.

Although further studies are necessary to test whether a deficiency in rRNA biogenesis is directly responsible for the malformations of CHARGE syndrome, an attractive hypothesis is that CHARGE is a 'ribopathy'. Indeed, several human genetic diseases are caused by mutations in genes that affect rRNA synthesis. Diamond-Blackfan anemia (DBA), characterized by a dramatic reduction in erythroid precursor cells as well as craniofacial, urogenital, cardiac and ophthalmologic defects, is caused by mutations in several genes that encode ribosomal proteins (42). The most frequently associated gene, *RPS19*, is mutated in ~25% of DBA cases and results in the decreased production of 18S rRNA and impaired maturation of the 40S ribosomal subunit (43). Most mutations detected in DBA are heterozygous, suggesting that haploinsufficiency is the underlying pathogenic mechanism (42). Another well-characterized genetic disorder resulting from impaired rRNA synthesis is TCS. Heterozygous mutations in the *TCOF1* gene, encoding the protein treacle, result in craniofacial anomalies, ear abnormalities and hearing loss due to deficiencies in rRNA biogenesis (39). As rRNA production is essential to all proliferating cell types, it is interesting that both of these disorders, like CHARGE syndrome, are characterized by cell type-specific defects. It is also noteworthy that DBA and TCS share some clinical features with CHARGE syndrome, including ear abnormalities and optic colobomata. Other notable conditions caused by mutations in nucleolar proteins include Bloom syndrome, Werner syndrome and Rothmund–Thomson syndrome. These diseases are caused by mutations in the genes encoding BLM, WRN and RECQL4 DNA helicases, respectively, which lead to genomic instability and predisposition to cancer (44). In contrast to CHD7, BLM, WRN and RECQL4 are not constitutively nucleolar; rather, they shuttle in and out of the nucleolus depending on cell cycle phase or conditions of stress (44), which might explain the phenotypic differences between these syndromes and more genuine 'ribopathies' such as TCS or DBA.

Interestingly, studies of haploinsufficient growth defects in non-mammalian model organisms also point to a large contribution of mutations in proteins with functions in ribosome biogenesis. A study of *Saccharomyces cerevisiae* heterozygous deletion strains revealed that ~3% of the yeast genome shows a haploinsufficient growth defect under conditions that favor rapid growth (45). Approximately 49% of the haploinsufficient genes identified were involved in ribosome biogenesis, when compared with ~4% for the next most-enriched category. This observation suggests that, in yeast, a primary outcome of haploinsufficiency is decreased protein synthesis.

In *Drosophila melanogaster*, the *Minute* mutations are a group of more than 50 distinct mutations, mostly in ribosomal proteins, that give rise to homozygous lethality and haploinsufficient growth defects such as short bristles, small body size and developmental delay (46). Finally, knockdown of 21 ribosomal proteins in zebrafish caused developmental phenotypes in the majority of cases (47). It therefore seems that genes that function in ribosome biogenesis are particularly dosage-sensitive.

How might CHD7 influence rRNA levels? CHD7 is thought to have chromatin remodeling activity owing to its SNF2-like ATPase/helicase domain. Thus, a likely scenario is that CHD7 either initiates or maintains open chromatin at active rDNA repeats to promote the association of factors involved in rRNA transcription. Consistent with this hypothesis, our results indicate that active rDNA becomes hypermethylated and less transcriptionally active upon reduction of CHD7 levels by siRNA-mediated knockdown or conventional knockout. ChIP studies of factors involved in rRNA transcription (such as RNA pol I or UBF) in the context of reduced CHD7 could be used to further test this hypothesis. In addition, CHD7 could play a role in antagonizing the repressive functions of the nucleolar remodeling complex (NoRC), which remodels chromatin and recruits DNA methyltransferases and histone deacetylases to rDNA (48). Nucleosome positioning at the promoter of mouse rDNA regulates CpG methylation (49). At transcriptionally active rDNA repeats, the promoter nucleosome covers nucleotides −157 to −2, confining CpG dinucleotides at positions −143 and −133 to the globular domain of the nucleosome. At inactive repeats, this nucleosome is shifted 25 nucleotides downstream, covering −132 to +22 and shifting the −143 and −133 CpGs to the linker region of the nucleosome, where they can then be methylated. NoRC induces sliding of this nucleosome to promote silencing of rDNA repeats via its SNF2-like ATPase subunit, Snf2h/Smarca5 (49). CHD7, via ATP-dependent chromatin remodeling, could position the promoter nucleosome in the active position, physically inhibiting DNA methylation. Studies of NoRC chromatin association and promoter nucleosome position in *Chd7* mutant cells are necessary to test this model.

One of the most puzzling issues surrounding the conditions that are caused by defects in ribosomal production and protein synthesis is cell type specificity. In TCS, haploinsufficiency of treacle results in a reduction in rRNA levels that ultimately affect the viability of neural crest cells, leading to the characteristic craniofacial anomalies of TCS. It is hypothesized that the basis for tissue specificity in TCS is related to the neural crest. Neural crest cells, which are multipotent and highly proliferative (50), utilize large amounts of energy for protein synthesis and proliferation, and as such may be particularly sensitive to perturbations in ribosome biogenesis. As this manuscript was under review, a study was published lending strong support to neural crest cells as the cell type of origin for many CHARGE-affected tissues (51). Based on these results, studies of rRNA biogenesis in CHD7-haploinsufficient neural crest cells could be informative with regard to linking the tissue-specific phenotypes of CHARGE to defects in rRNA biogenesis.

Our studies define a novel function for CHD7 in rRNA synthesis. Future studies will focus on testing whether the dysregulated expression of rRNA alone, or in combination with dysregulated nucleoplasmic gene expression, contributes to the pathogenesis of CHARGE syndrome. To distinguish between these possibilities, mice with mutations in known negative regulators of rRNA transcription such as Tip5 or Fbxl10 (28, 29) could be bred to *Chd7*-mutant mice to examine whether the restoration of rRNA synthesis rescues the CHARGE-like phenotype. Genetic crosses between *Chd7* mutants and mice harboring mutations in positive regulators of rRNA biogenesis, such as *Tcof1*, could also be worthwhile, as an exacerbation of the phenotype could highlight epistatic interactions.

MATERIALS AND METHODS

Cell culture, siRNA knockdown, and CHD7 overexpression

DLD1-A2 and mES cells were cultured as previously described (15). Non-target and CHD7 siRNA Smartpools were purchased from Dharmacon. An additional CHD7 siRNA not present in the Smartpool was purchased from Sigma. CHD7 mRNA and protein levels were assessed ∼72 h after transfection with qRT–PCR and western blotting. For overexpression, empty pCI-neo (Promega) or pCI-neo containing untagged full-length human CHD7 was transfected into DLD1-A2 cells, which express only FLAG-tagged CHD7. Protein and RNA were harvested ∼72 h after transfection for the analysis of CHD7 protein expression and 45S pre-rRNA levels. Endogenous FLAG-tagged CHD7 was detected with mouse anti-FLAG M5 (Sigma, 1:1000) and transfected untagged CHD7 was detected with rabbit anti-CHD7 (Abcam ab31824, 1:1000), which does not detect the FLAG-tagged protein (see Supplementary Material, Fig. S2 for details).

Indirect immunofluorescence

DLD1-A2 cells were grown overnight on glass cover slips and fixed in cold 4% paraformaldehyde in PBS for 15 min at RT. Cells were washed with PBS and permeabilized with 0.2% Triton X-100 in PBS for 5 min at RT. Cells were washed with PBS and blocked with 10% normal goat serum in PBS for 30 min at RT. Cells were incubated with primary antibodies overnight at 4°C. Cells were washed with PBS and incubated with secondary antibodies for 1 h at RT. Cells were washed, mounted and visualized on a Leica DM6000 upright microscope with Volocity 4.4 software. Antibodies used for immunofluorescence were mouse anti-FLAG M5 (Sigma, 1:500), rabbit anti-nucleolin (Abcam ab22758, 1:500), AlexaFluor goat anti-mouse 488 (Invitrogen, 1:200), and AlexaFluor goat anti-rabbit 594 (Invitrogen, 1:200).

Nucleolar isolation and western blotting

Nucleoli were isolated using a modified version (52) of an established protocol (53). Forty micrograms of cytoplasmic, nucleoplasmic and nucleolar protein was separated by SDS–PAGE and detected by western blotting. Antibodies used for western blotting were mouse anti-FLAG M5 (Sigma, 1:1000), rabbit anti-CHD7 (Abcam ab31824), mouse anti-NUP62 (Abcam ab56982, 1:1000), rabbit anti-UBF (Bethyl Labs BL859-301, 1:5000), rabbit anti-treacle (Abcam ab65212, 1:750), mouse

anti-p53 (Santa Cruz sc-126, 1:250) and rabbit anti-tubulin (ICN BioMedicals, 1:5000).

Cell proliferation analysis

DLD1-A2 cells were transfected with control or CHD7 siRNA as described. For cell counting, cells were plated in triplicate in a 24-well plate. Wells were counted in duplicate every 24 h using the Countess Automated Cell Counter (Invitrogen). For BrdU labeling, the *In Situ* Cell Proliferation Kit FLUOS (Roche) was used. Briefly, cells grown on cover slips were pulsed with 10 μM BrdU for 30 min at 37°C. Cells were fixed for 45 min with 7 volumes 100% ethanol:3 volumes 50 mM glycine, pH 2.0 at RT. DNA was denatured for 15 min with 4 M HCl and pH was neutralized with excess incubation buffer at RT. Cells were incubated with anti-BrdU-FLUOS antibody for 30 min at 37°C in the dark. Cells were processed for immunofluorescence and viewed as described above. For the quantitative analysis of proliferation, four to five separate fields from each cover slip were analyzed using the Cell Counter plugin for ImageJ. Between 600 and 1200 cells were counted per cover slip.

Metabolic labeling

Cells were transfected with siRNA as indicated above. On the indicated days post-transfection, cells were pulsed for 30 min with 0.03 mCi/ml [^{35}S]methionine (EasyTag Express Protein Labeling Mix, PerkinElmer). The unincorporated [^{35}S]methionine was chased with 5% TCA/1 mM cold methionine and cells were solubilized with 1 N NaOH/0.5% DOC. Counts were determined by scintillation and normalized to total protein as measured by the Lowry assay.

qRT–PCR

RNA was extracted from cells with TRIzol (Invitrogen) or mouse tissues with the RNAqueous-Micro kit (Ambion) and cDNA was synthesized using the High-Capacity cDNA Archive Kit (ABI). qRT–PCR reactions were performed in triplicate on a GeneAmp 7300 real-time thermal cycler (ABI) using Sybr Green chemistry. *GAPDH* was used as an endogenous control for all qRT–PCR reactions. Primer sequences are available upon request.

Chromatin immunoprecipitation

ChIP was performed as previously described (15). Antibodies used for ChIP were mouse anti-FLAG M5 (Sigma), rabbit anti-CHD7 (Abcam ab31824), goat anti-H3K4me2 (Abcam ab11946), mouse anti-H3K9me2 (Abcam ab1220) and rabbit anti-treacle (Abcam ab65212). Primer sequences are available upon request. All rDNA primers except the pair amplifying the 41 kb region of mouse rDNA have been previously described to amplify sufficiently complex regions to yield a single product (54) and all primers gave a single product in a dissociation step.

ChIP-seq

ChIP-seq was performed according to a published protocol (55). ChIP-seq data for input and IP samples from DLD1-A2 or mES cells was aligned with MAQ (56) to the human (GenBank accession no. U13369) or mouse rDNA repeat (GenBank accession no. BK000964). The input signal was subtracted from the IP signal at each base to obtain a plot of relative enrichment using the R statistical package.

ChIP-chop

ChIP was performed as described, except that before qPCR was performed, aliquots of input and ChIP DNA were digested with *Hpa*II. ChIPs were normalized to input and *Hpa*II resistance was determined by normalizing the digested DNA to mock-digested DNA.

rDNA promoter methylation analysis

Genomic DNA from DLD1-A2 or mES cells was digested with *Hpa*II and analyzed by qPCR. *Hpa*II resistance was calculated by normalizing digests to mock-digested DNA. Genomic DNA was also digested with *Msp*I to ensure that the results of the *Hpa*II digests could be interpreted in the content of CpG methylation within the CCGG sequence.

SUPPLEMENTARY MATERIAL

Supplementary Material is available at *HMG* online.

ACKNOWLEDGEMENTS

We thank Helen Salz for critical reading of the manuscript and Stephanie Balow for technical assistance.

Conflict of Interest statement. None declared.

FUNDING

This work was supported by the National Institute of General Medical Sciences (5T32GM008613-14 to G.E.Z.), the National Institute of Diabetes and Digestive and Kidney Diseases (DK60596 to M.H.), the National Institutes of Health (R01DC009410 and R01NS054784 to D.M.M.), the National Institute of Child Health and Development (R01HD056369 to P.C.S.) and the National Human Genome Research Institute (5R01HG004722 to P.C.S.).

REFERENCES

1. Hall, J.A. and Georgel, P.T. (2007) CHD proteins: a diverse family with strong ties. *Biochem. Cell Biol.*, **85**, 463–476.
2. Marfella, C.G.A. and Imbalzano, A.N. (2007) The Chd family of chromatin remodelers. *Mutat. Res.*, **618**, 30–40.
3. Gaspar-Maia, A., Alajem, A., Polesso, F., Sridharan, R., Mason, M.J., Heidersbach, A., Ramalho-Santos, J., McManus, M.T., Plath, K., Meshorer, E. *et al.* (2009) Chd1 regulates open chromatin and pluripotency of embryonic stem cells. *Nature*, **460**, 863–868.
4. Denslow, S.A. and Wade, P.A. (2007) The human Mi-2/NuRD complex and gene regulation. *Oncogene*, **26**, 5433–5438.
5. Bagchi, A., Papazoglu, C., Wu, Y., Capurso, D., Brodt, M., Francis, D., Bredel, M., Vogel, H. and Mills, A.A. (2007) CHD5 is a tumor suppressor at human 1p36. *Cell*, **128**, 459–475.
6. Rodriguez-Paredes, M., Ceballos-Chavez, M., Esteller, M., Garcia-Dominguez, M. and Reyes, J.C. (2009) The chromatin remodeling

factor CHD8 interacts with elongating RNA polymerase II and controls expression of the cyclin E2 gene. *Nucleic Acids Res.*, **37**, 2449–2640.
7. Thompson, B.A., Tremblay, V., Lin, G. and Bochar, D.A. (2008) CHD8 is an ATP-dependent chromatin remodeling factor that regulates β-catenin target genes. *Mol. Cell. Biol.*, **28**, 3894–3904.
8. Zentner, G.E., Layman, W.S., Martin, D.M. and Scacheri, P.C. (2010) Molecular and phenotypic aspects of *CHD7* mutation in CHARGE syndrome. *Am. J. Med. Genet. A*, **152A**, 674–686.
9. Jongmans, M.C., Admiraal, R.J., van der Donk, K.P., Vissers, L.E., Baas, A.F., Kapusta, L., van Hagen, J.M., Donnai, D., de Ravel, T.J., Veltman, J.A. *et al.* (2006) CHARGE syndrome: the phenotypic spectrum of mutations in the *CHD7* gene. *J. Med. Genet.*, **43**, 306–314.
10. Van de Laar, I., Dooijes, D., Hoefsloot, L., Simon, M., Hoogeboom, J. and Devriendt, K. (2007) Limb anomalies in patients with CHARGE syndrome: an expansion of the phenotype. *Am. J. Med. Genet. A*, **143A**, 2712–2715.
11. Layman, W.S., McEwen, D.P., Beyer, L.A., Lalani, S.R., Fernbach, S.D., Oh, E., Swaroop, A., Hegg, C.C., Raphael, Y., Martens, J.R. *et al.* (2009) Defects in neural stem cell proliferation and olfaction in *Chd7* deficient mice indicate a mechanism for hyposmia in human CHARGE syndrome. *Hum. Mol. Genet.*, **18**, 1909–1923.
12. Bosman, E.A., Penn, A.C., Ambrose, J.C., Kettleborough, R., Stemple, D.L. and Steel, K.P. (2005) Multiple mutations in mouse *Chd7* provide models for CHARGE syndrome. *Hum. Mol. Genet.*, **14**, 3463–3476.
13. Bergman, J.E.H., Bosman, E.A., van Ravenswaaij-Arts, C.M.A. and Steel, K.P. (2010) Study of smell and reproductive organs in a mouse model for CHARGE syndrome. *Eur. J. Hum. Genet.*, **18**, 171–177.
14. Hurd, E., Capers, P., Blauwkamp, M., Adams, M., Raphael, Y., Poucher, H. and Martin, D. (2007) Loss of *Chd7* function in gene-trapped reporter mice is embryonic lethal and associated with severe defects in multiple developing tissues. *Mamm. Genome*, **18**, 94–104.
15. Schnetz, M.P., Bartels, C.F., Shastri, K., Balasubramanian, D., Zentner, G.E., Balaji, R., Song, L., Wang, Z., LaFramboise, T., Crawford, G.E. *et al.* (2009) Genomic distribution of CHD7 on chromatin tracks H3K4 methylation patterns. *Genome Res.*, **19**, 590–601.
16. Schnetz, M.P., Handoko, L., Akhtar-Zaidi, B., Bartels, C.F., Pereira, C.F., Fisher, A.G., Adams, D., Flicek, P., Crawford, G.E., LaFramboise, T. *et al.* (2010) CHD7 modulates ES cell-specific gene expression by targeting active gene enhancer elements. *PLoS Genet.*, in press.
17. Ahmad, Y., Boisvert, F.-M., Gregor, P., Cobley, A. and Lamond, A.I. (2009) NOPdb: Nucleolar Proteome Database—2008 update. *Nucleic Acids Res.*, **37**, D181–D184.
18. Shimono, K., Shimono, Y., Shimokata, K., Ishiguro, N. and Takahashi, M. (2005) Microspherule protein 1, Mi-2β, and RET finger protein associate in the nucleolus and up-regulate ribosomal gene transcription. *J. Biol. Chem.*, **280**, 39436–39447.
19. Zhang, X., Guo, C., Chen, Y., Shulha, H.P., Schnetz, M.P., LaFramboise, T., Bartels, C.F., Markowitz, S., Weng, Z., Scacheri, P.C. *et al.* (2008) Epitope tagging of endogenous proteins for genome-wide ChIP–chip studies. *Nat. Methods*, **5**, 163–165.
20. Mongelard, F. and Bouvet, P. (2007) Nucleolin: a multiFACeTed protein. *Trends Cell Biol.*, **17**, 80–86.
21. McStay, B. and Grummt, I. (2008) The epigenetics of rRNA genes: from molecular to chromosome biology. *Annu. Rev. Cell Dev. Biol.*, **24**, 131–157.
22. Henderson, A., Warburton, D. and Atwood, K. (1972) Location of ribosomal DNA in the human chromosome complement. *Proc. Natl Acad. Sci. USA*, **69**, 3394–3398.
23. Dev, V., Tantravahi, R., Miller, D. and Miller, O. (1977) Nucleolus organizers in *Mus musculis* subspecies and in the RAG mouse cell line. *Genetics*, **86**, 389–398.
24. Bakshi, R., Zaidi, S.K., Pande, S., Hassan, M.Q., Young, D.W., Montecino, M., Lian, J.B., van Wijnen, A.J., Stein, J.L. and Stein, G.S. (2008) The leukemogenic t(8;21) fusion protein AML1-ETO controls rRNA genes and associates with nucleolar-organizing regions at mitotic chromosomes. *J. Cell Sci.*, **121**, 3981–3990.
25. Ali, S., Zaidi, S., Dacwag, C., Salma, N., Young, D., Shakoori, A., Monecino, M., Lian, J., van Wijnen, A., Imbalzano, A. *et al.* (2008) Phenotypic transcription factors epigenetically mediate cell growth control. *Proc. Natl Acad. Sci. USA*, **105**, 6632–6637.
26. Sanij, E. and Hannan, R.D. (2009) The role of UBF in regulating the structure and dynamics of transcriptionally active rRNA chromatin. *Epigenetics*, **4**, 374–382.
27. Fromont-Racine, M., Senger, B., Saveanu, C. and Fasiolo, F. (2003) Ribosome assembly in eukaryotes. *Gene*, **313**, 17–42.
28. Frescas, D., Guardavaccaro, D., Bassermann, F., Koyama-Nasu, R. and Pagano, M. (2007) JHDM1B/FBXL10 is a nucleolar protein that represses transcription of ribosomal RNA genes. *Nature*, **450**, 309–313.
29. Li, J., Santoro, R., Koberna, K. and Grummt, I. (2005) The chromatin remodeling complex NoRC controls replication timing of rRNA genes. *EMBO J.*, **24**, 120–127.
30. Feng, W., Yonezawa, M., Ye, J., Jenuwein, T. and Grummt, I. (2010) PHF8 activates transcription of rRNA genes through H3K4me3 binding and H3K9me1/2 demethylation. *Nat. Struct. Mol. Biol.*, **17**, 445–450.
31. Chédin, S., Laferté, A., Hoang, T., LaFontaine, D., Riva, M. and Carles, C. (2007) Is ribosome synthesis controlled by pol I transcription? *Cell Cycle*, **6**, 11–15.
32. Opferman, J.T. and Zambetti, G.P. (2006) Translational research? Ribosome integrity and a new p53 tumor suppressor checkpoint. *Cell Death Differ.*, **13**, 898–901.
33. Huo, J.X., Metz, S.A. and Li, G.D. (2003) p53-Independent induction of p21waf1//cip1 contributes to the activation of caspases in GTP-depletion-induced apoptosis of insulin-secreting cells. *Cell Death Differ.*, **11**, 99–109.
34. Aliouat-Denis, C.-M., Dendouga, N., Van den Wyngaert, I., Goehlmann, H., Steller, U., van de Weyer, I., Van Slycken, N., Andries, L., Kass, S., Luyten, W. *et al.* (2005) p53-Independent regulation of p21Waf1/Cip1 expression and senescence by Chk2. *Mol. Cancer Res.*, **3**, 627–634.
35. Sankala, H.M., Hait, N.C., Paugh, S.W., Shida, D., Lepine, S., Elmore, L.W., Dent, P., Milstien, S. and Spiegel, S. (2007) Involvement of sphingosine kinase 2 in p53-independent induction of p21 by the chemotherapeutic drug doxorubicin. *Cancer Res.*, **67**, 10466–10474.
36. Megyesi, J., Udvarhelyi, N., Safirstein, R.L. and Price, P.M. (1996) The p53-independent activation of transcription of p21 WAF1/CIP1/SDI1 after acute renal failure. *Am. J. Physiol. Renal Physiol.*, **271**, F1211–F1216.
37. Abbas, T. and Dutta, A. (2009) p21 in cancer: intricate networks and multiple activities. *Nat. Rev. Cancer*, **9**, 400–414.
38. Zhou, Y., Schmitz, K.-M., Mayer, C., Yuan, X., Akhtar, A. and Grummt, I. (2009) Reversible acetylation of the chromatin remodelling complex NoRC is required for non-coding RNA-dependent silencing. *Nat. Cell Biol.*, **11**, 1010–1016.
39. Dixon, J., Trainor, P. and Dixon, M.J. (2007) Treacher Collins syndrome. *Orthod. Craniofac. Res.*, **10**, 88–95.
40. Valdez, B.C., Henning, D., So, R., Dixon, J. and Dixon, M.J. (2004) The Treacher Collins syndrome (*TCOF1*) gene product is involved in ribosomal DNA gene transcription by interacting with upstream binding factor. *Proc. Natl Acad. Sci. USA*, **101**, 10709–10714.
41. Raška, I., Koberna, K., Malínský, J., Fidlerová, H. and Mašata, M. (2004) The nucleolus and transcription of ribosomal genes. *Biol. Cell*, **96**, 579–594.
42. Vlachos, A., Ball, S., Dahl, N., Alter, B.P., Sheth, S., Ramenghi, U., Meerpohl, J., Karlsson, S., Liu, J.M., Leblanc, T. *et al.* (2008) Diagnosing and treating Diamond–Blackfan anaemia: results of an international clinical consensus conference. *Br. J. Haematol.*, **142**, 859–876.
43. Choesmel, V., Bacqueville, D., Rouquette, J., Noaillac-Depeyre, J., Fribourg, S., Cretien, A., Leblanc, T., Tchernia, G., Da Costa, L. and Gleizes, E. (2007) Impaired ribosome biogenesis in Diamond–Blackfan anemia. *Blood*, **109**, 1275–1283.
44. Boisvert, F.-M., van Koningsbruggen, S., Navascues, J. and Lamond, A.I. (2007) The multifunctional nucleolus. *Nat. Rev. Mol. Cell. Biol.*, **8**, 574–585.
45. Deutschbauer, A.M., Jaramillo, D.F., Proctor, M., Kumm, J., Hillenmeyer, M.E., Davis, R.W., Nislow, C. and Giaver, G. (2005) Mechanisms of haploinsufficiency revealed by genome-wide profiling in yeast. *Genetics*, **169**, 1915–1925.
46. Marygold, S., Roote, J., Reuter, G., Lambertsson, A., Ashburner, M., Millburn, G., Harrison, P., Yu, Z., Kenmochi, N., Kaufman, T. *et al.* (2007) The ribosomal protein genes and Minute loci of *Drosophila melanogaster*. *Genome Biol.*, **8**, R216.
47. Uechi, T., Nakajima, Y., Nakao, A., Torihara, H., Chakraborty, A., Inoue, K. and Kenmochi, N. (2006) Ribosomal protein gene knockdown causes developmental defects in zebrafish. *PLoS ONE*, **1**, e37.
48. Santoro, R., Li, J. and Grummt, I. (2002) The nucleolar remodeling complex NoRC mediates heterochromatin formation and silencing of ribosomal gene transcription. *Nat. Genet.*, **32**, 393–396.

49. Li, J., Langst, G. and Grummt, I. (2006) NoRC-dependent nucleosome positioning silences rRNA genes. *EMBO J.*, **25**, 5735–5741.
50. Lo, L. and Anderson, D.J. (1995) Postmigratory neural crest cells expressing c-RET display restricted developmental and proliferative capacities. *Neuron*, **15**, 527–539.
51. Bajpai, R., Chen, D.A., Rada-Iglesias, A., Zhang, J., Xiong, Y., Helms, J., Chang, C.-P., Zhao, Y., Swigut, T. and Wysocka, J. (2010) CHD7 cooperates with PBAF to control multipotent neural crest formation. *Nature*, **463**, 958–962.
52. Andersen, J.S., Lyon, C.E., Fox, A.H., Leung, A.K.L., Lam, Y.W., Steen, H., Mann, M. and Lamond, A.I. (2002) Directed proteomic analysis of the human nucleolus. *Curr. Biol.*, **12**, 1–11.
53. Muramatsu, M., Smetana, K. and Busch, H. (1963) Quantitative aspects of isolation of nucleoli of the Walker carcinosarcoma and liver of the rat. *Cancer Res.*, **25**, 693–697.
54. O'Sullivan, A.C., Sullivan, G.J. and McStay, B. (2002) UBF binding *in vivo* is not restricted to regulatory sequences within the vertebrate ribosomal DNA repeat. *Mol. Cell. Biol.*, **22**, 657–658.
55. Schmidt, D., Wilson, M.D., Spyrou, C., Brown, G.D., Hadfield, J. and Odom, D.T. (2009) ChIP-seq: Using high-throughput sequencing to discover protein–DNA interactions. *Methods*, **48**, 240–248.
56. Li, H., Ruan, J. and Durbin, R. (2008) Mapping short DNA sequencing reads and calling variants using mapping quality scores. *Genome Res.*, **18**, 1851–1858.